PHYSICAL REVIEW A VOLUME 21, NUMBER 6 JUNE 1980

Effects of velocity-changing collisions on two-photon and stepwise-absorption spectroscopic line shapes

P. F. Liao and J. E. Bjorkholm
Bell Laboratories, Holmdel, New Jersey 07733

P. R. Berman
Physics Department, New York University, New York, New York 10003

(Received 5 September 1979)

We report the results of an experimental study of the effects of velocity-changing collisions on two-photon and stepwise-absorption line shapes. Excitation spectra for the $3S_{1/2}\rightarrow 3P_{1/2}\rightarrow 4D_{3/2}$ transitions of sodium atoms undergoing collisions with foreign gas perturbers are obtained. These spectra are obtained with two cw dye lasers. One laser, the pump laser, is tuned 1.6 GHz below the $3S_{1/2}\rightarrow 3P_{1/2}$ transition frequency and excites a nonthermal longitudinal velocity distribution of excited $3P_{1/2}$ atoms in the vapor. Absorption of the second (probe) laser is used to monitor the steady-state excited-state distribution which is a result of collisions with rare gas atoms. The spectra are obtained for various pressures of He, Ne, and Kr gases and are fit to a theoretical model which utilizes either the phenomenological Keilson-Störer or the classical hard-sphere collision kernel. The theoretical model includes the effects of collisionally aided excitation of the $3P_{1/2}$ state as well as effects due to fine-structure state-changing collisions. Although both kernels are found to predict line shapes which are in reasonable agreement with the experimental results, the hard-sphere kernel is found superior as it gives a better description of the effects of large-angle scattering for heavy perturbers. Neither kernel provides a fully adequate description over the entire line profile. The experimental data is used to extract effective hard-sphere collision cross sections for collisions between sodium $3P_{1/2}$ atoms and helium, neon, and krypton perturbers.

I. INTRODUCTION

Using tunable narrow-band lasers, one can selectively excite a narrow nonthermal longitudinal velocity distribution in an atomic or molecular vapor. Collisions between these atoms or molecules and other atoms in the gas cause this distribution to thermalize. A study of the manner in which the collisions modify the distribution leads to an increased understanding of the collisions. In this paper we report the results of a systematic study of the effects of collisions on line shapes obtained in sodium using two-photon spectroscopy with a resonant intermediate state. These measurements, which are made with two cw dye lasers, yield values for the equivalent hard-sphere elastic-scattering cross sections for collisions between sodium atoms in the $3P_{1/2}$ state and rare gas perturbers. Comparisons of the experimental line shapes are made with a theory which utilizes either a classical hard-sphere collision kernel or the Keilson-Störer collision kernel. The theory accounts for the presence of fine-structure state-changing collisions as well as velocity-changing collisions. The validity of these collision models is discussed in light of the experimental data.

Measurements of the effects of velocity-changing collisions on laser spectroscopic line shapes have been made for some time.[1,2] In a typical experiment, one monitors the steady-state velocity distribution of atomic levels subjected to nonthermal excitation by a narrow-band laser. The degree of velocity thermalization achieved in these states as a result of collisions is determined by the number of collisions occurring within the lifetime of the states and the strength of the collisions. Most previous experiments have been analyzed under the assumptions that the collisions are either of a "weak" or "strong" nature. In the case of "weak" collisions, the collisions which occur during an atom's lifetime have only a small effect on the atomic velocity,[3] whereas, in the "strong" collision limit, those atoms which have experienced collisions are assumed to have a thermal distribution. Recently the problem of collisions intermediate to the two limits has received increased attention.[2] In this case, atoms which experience collisions reach a thermal velocity distribution only if they have several collisions within their lifetime. Because of the short lifetime of the excited atoms in our experiment (16 nsec), the excited sodium atoms never reach a thermal distribution so that the measured steady-state velocity distribution shows a "persistence of velocity."

The manner in which the atoms change velocities as a result of collisions is directly dependent on the strength and form of the interaction between the active atom and the perturber atom.

Hence, measurements of the thermalization process yield information about the interaction potentials. At the present time we have analyzed our experimental results to obtain the equivalent hard-sphere cross sections for sodium in collision with helium, neon, or krypton rare gas atoms. This choice of perturber atoms allows us to observe the effect of different active atom to perturber atom mass ratios.

Our measurements are made by selectively exciting a particular velocity distribution of sodium atoms to the $3P_{1/2}$ excited state. This excitation is accomplished by tuning a cw dye laser to the wing of the Doppler-broadened $3S_{1/2} - 3P_{1/2}$ transition. A second laser is then scanned to produce $3P_{1/2}$-$4D_{3/2}$ transitions. The resulting line shape directly reflects the longitudinal velocity distribution of the $3P_{1/2}$ state.

In the absence of velocity-changing collisions, one might expect only those atoms which have longitudinal velocities such that they are Doppler shifted into resonance with the laser frequency would be excited. However, the presence of phase-interrupting collisions results in an excitation of all the velocity groups. In this nonresonant excitation, the energy defect or excess between the atomic transition energy and the laser photon energy is provided or removed by a collision.[4,5] This nonresonant collisionally assisted excitation results in population of velocity groups other than those desired and must be accounted for properly in the final analysis of the line shape.

State-changing collisions such as those which produce transitions between the $3P_{1/2}$ and $3P_{3/2}$ fine-structure states are also found to play an important role. Our analysis is therefore made to account for the effects of such collisions.

In the following section we briefly discuss our experimental setup and the underlying principles involved in obtaining a description of the collision-induced modification of spectroscopic line shapes. In Sec. III we compare two kernels (Keilson-Störer[6] and classical hard sphere) that can be used to describe velocity-changing collisions. Our experimental results and a comparison with theory using these collision kernels are then discussed in Sec. IV.

II. BASIC PRINCIPLES AND EXPERIMENTAL SETUP

The effect of collisions on the line shapes associated with three-level systems has been treated recently[7] and the following discussion will be based largely on those results. Our experimental situation is, in fact, somewhat more complicated than the simple three-level case due to the presence of additional levels. While these additional levels are not coupled by the laser radiation fields to the other states, collisions can cause transitions between these levels and the states of interest. Furthermore, the theory given in Ref. 7 is valid only in the limit of low intensities. Our actual experiment utilized intensities which often exceed the saturation intensity of a transition and require a more accurate theory to completely describe it. A detailed discussion of this more complete theory is given elsewhere.[8] In what follows, we give only an outline of the basic principles of the experiment and present the major theoretical results.

Our experimental data are obtained using the experimental setup shown in Fig. 1. We use two cw single-mode dye lasers; one (the pump) is set at a fixed angular frequency Ω which is tuned to the wing of the Doppler-broadened $3S_{1/2}$-$3P_{1/2}$ transition, and the other (the probe), of frequency Ω', is scanned to complete transitions to the $4D_{3/2}$ state. Transitions to $4D_{5/2}$ are weak in comparison with those to $4D_{3/2}$, because of dipole selection rules which forbid $3P_{1/2} \rightarrow 4D_{5/2}$ transitions, and are neglected. The unfocused beams from the two lasers propagate in opposite directions through a cell at 200 °C containing sodium vapor. Typical laser intensities are 0.5 W/cm^2, and each beam is linearly polarized in the same direction. The sodium vapor density is held between 10^{10}–10^{11} cm^{-3} so that resonant reabsorption of atomic fluorescence was not significant and sodium-sodium collisions could be neglected. We monitor the population of the $4D_{3/2}$ state by measuring the intensity of fluorescence at ~330 nm which occurs when the $4D_{3/2}$ state decays via the $4P$ state back to the ground state. Our results give

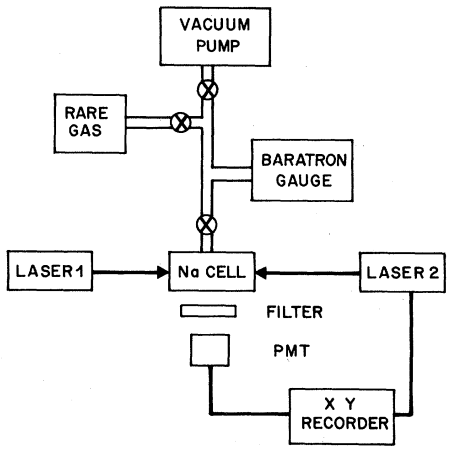

FIG. 1. Schematic diagram of the experimental setup. Although not shown, the light from laser 1 was chopped and the output of the photomultiplier (PMT) was processed with a lock-in amplifier.

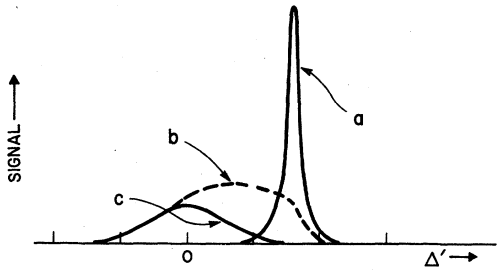

FIG. 2. Schematic representation of the observed line shape in terms of three components. Component (a) is the "two-photon" line; components (b) and (c) are the collisionally induced components, as discussed in the text.

the $3S_{1/2} - 3P_{1/2} - 4D_{3/2}$ two-photon excitation spectrum.

The line shape can be roughly viewed as composed of three parts which are illustrated schematically in Fig. 2. Although the three components are not completely independent, one can roughly describe them as arising in the following manner. The narrow component marked a would be present even in the absence of collisions and is composed of two-quantum and stepwise transitions of those atoms which have not undergone velocity-changing collisions in the $3P_{1/2}$ intermediate state. We shall refer to this component as the "two-photon" line. The characteristics of this line have been experimentally[9] and theoretically[10] studied in great detail. The line is essentially Doppler free owing to the velocity selectivity of the excitation and the use of oppositely propagating beams. The component labeled b arises from those atoms which, once excited into the $3P_{1/2}$ state, experience velocity-changing collisions. The collisions modify the initial narrow velocity distribution which was excited by the laser at frequency Ω and cause the distribution to broaden and shift toward equilibrium; this thermalization is mirrored in component b of the probe absorption. In our experiments Ω is not set at the atomic resonance frequency and hence the initial longitudinal velocity distribution is not centered at $v_z = 0$ but at a fairly high $v_z \approx 10^5$ cm/sec. The final component, labeled c, is due to collisionally aided excitation of the $3P_{1/2}$ excited state. This excitation is essentially non-velocity-selective and therefore is completely Doppler broadened; the probe absorption from this state has nearly the shape of the equilibrium Voigt profile. It differs from the velocity-changing collision component, b, as it would be present even in the absence of velocity-changing collisions, e.g., if the perturber atoms were much less massive than the sodium atoms. It may be viewed as arising from phase-changing collisions

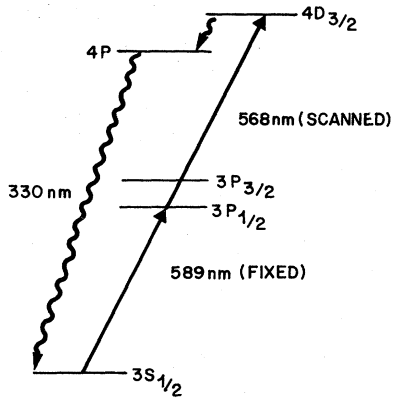

FIG. 3. The energy levels of the sodium atom relevant for our experiment. Not shown is the 1.77-GHz hyperfine splitting of the 3S ground state.

which effectively broaden the atomic resonance of each atom. The exact shape of the excitation spectrum depends on the relative amplitudes of the three components. The components b and c each increase relative to a as the perturber pressure is increased. The ratio of b to c amplitudes depends on Ω. Component b decreases rapidly when Ω is adjusted away from the atomic resonance because the number of atoms which have the correct velocity so as to be Doppler shifted into resonance decreases exponentially. Hence at detunings much greater than the Doppler width, component c will dominate, while at small detunings component b will dominate. We have recently made a detailed study of the collisional redistribution by phase-changing collisions for the case where Ω is tuned far from the resonance so that component b is negligible.[5]

The level scheme which is appropriate for our experiments is shown in Fig. 3. We generally follow the notation of Refs. 7 and 8 so that state 1 is the $3S_{1/2}$ ground state, state 3 is the $4D_{3/2}$ final state, and state 2 is the $3P_{1/2}$ intermediate state. We also allow for state-changing collisions between the $3P_{1/2}$ and $3P_{3/2}$ (state 4) fine-structure states. The laser field at Ω' is assumed to couple only the $2 \leftrightarrow 3$ transition, while that at Ω is assumed to act on only the $1 \leftrightarrow 2$ transition.

A complete theory for the excitation line shape is given in Ref. 8 assuming the probe field to be weak. We shall attempt to fit our data using this theory and hard-sphere collision models. For such models, collisions produce relatively large velocity changes for the active atoms [i.e., velocity changes Δu such that $\Omega(\Delta u/c) \gtrsim$ all homogeneous widths]. In this limit the line shape is given by[8]

$$I(\Omega') = I_{TQ}(\Omega') + I_{SW}(\Omega'), \quad (1)$$

where

$$I_{TQ}(\Omega') = \frac{2(\chi'\chi)^2}{\gamma_3 k k' k'' u^3} \mathrm{Im} \sum_{j=1}^{4} A_j \tilde{Z}(r_j), \tag{2}$$

$$I_{SW}(\Omega') = \frac{2(\chi')^2}{\gamma_3 k'} \mathrm{Im} \int \frac{n_2(ux)}{(x - r_2)} dx, \tag{3}$$

$$\tilde{Z}(r) = -\pi^{-1/2} \int_{-\infty}^{\infty} e^{-x^2} (r - x)^{-1} dx$$

[$\tilde{Z}(r)$ is the plasma dispersion function $Z(r)$ for $\mathrm{Im}(r) > 0$ and is $-Z(r)$ for $\mathrm{Im}(r) < 0$], where $\chi(\chi')$ is the Rabi frequency of the transition $1 \rightarrow 2$ ($2 \rightarrow 3$), u is the most probable sodium velocity, $k = \Omega/c$, $k' = \Omega'/c$, and $k'' = |k' - k|$. The other quantities are defined as

$$r_1 = a + c,$$

$$r_2 = b - c,$$

$$r_3 = i\eta_B/ku,$$

$$r_4 = -i\eta_B/ku,$$

$$r_5 = i\eta_{12}^*/ku,$$

where

$$a = \frac{+i\eta_{13}}{k''u}, \quad b = \frac{i\eta_{23}}{k'u},$$

$$c = \tfrac{1}{2}\{b - a - [(b - a)^2 + 4\chi^2/k'k''u^2]^{1/2}\},$$

and

$$A_i = (r_5 - r_i) \Big/ \prod_{j=1,4;\, j\neq i} (r_j - r_i),$$

$$\eta_{12} = \tilde{\gamma}_{12} + i\Delta,$$

$$\eta_{13} = \tilde{\gamma}_{13} + i(\Delta + \Delta'),$$

$$\eta_{23} = \tilde{\gamma}_{23} + i\Delta',$$

$$\eta_B = \gamma_B + i\Delta, \quad (\gamma_B)^2 = \tilde{\gamma}_{12}^2 + 2\tilde{\gamma}_{12}\chi^2/\Gamma_S,$$

$$\Gamma_S^{-1} = \frac{\gamma_2 + \Gamma_2(v) + 0.5\gamma^t}{[\gamma_2 + \Gamma_2(v)][\gamma_2 + \Gamma_2(v) + 1.5\gamma^t]} + \frac{1}{\Gamma_1(v)}\left(1 - \frac{\gamma_2'}{\gamma_2 + \Gamma_2(v)}\right).$$

The detunings are defined as $\Delta = \Omega - \omega$, $\Delta' = \Omega' - \omega'$, where the angular frequencies ω and ω' are the transition frequencies of the ground-to-intermediate and intermediate-to-final states, respectively. The decay rates $\tilde{\gamma}_{ij}$ are the phenomenological decay constants of the density matrix elements ρ_{ij} and include the effects of phase-changing collisions. The rate γ_2 is the total natural decay rate out of the intermediate state, γ_2' is the natural decay rate from level 2 to 1, $\Gamma_i(v)$ is the rate of velocity-changing collisions for atoms in level i, and γ^t is the $3P_{1/2}$ to $3P_{3/2}$ fine-structure state-changing collision rate. Note that the theory allows for power broadening of the $1 \rightarrow 2$ transition. The population distribution $n_2(v)$ of the intermediate state appearing in Eq. (3) is determined by the atom-pump field interaction and the effects of velocity-changing collisions. Equation (3) is an approximation valid for the case $|k| \approx |k'|$ as in our experiment.

The effect of fine-structure state-changing collisions introduces additional complexities. First, it modifies the power broadening of the $1 \rightarrow 2$ transition. Second, it may modify the velocity-changing process. Finally, it decreases the effective excitation of state 2 since atoms are transferred from the $3P_{1/2}$ to the $3P_{3/2}$ state. To minimize the complexities we make the simplifying assumption that the velocity-changing cross section is the same for the two fine-structure states, and that no velocity change occurs in the fine-structure state-changing processes. We have verified that the latter assumption is nearly correct by tuning Ω to the wing of the $3S_{1/2} \rightarrow 3P_{3/2}$ transition and thereby exciting a particular velocity class of atoms into the $3P_{3/2}$ state. Collisions cause some of these atoms to transfer to the $3P_{1/2}$ state. The velocity distribution of the atoms in the $3P_{1/2}$ state is then recorded by scanning Ω' across the region of the $3P_{1/2} \rightarrow 4D_{3/2}$ transition. The resulting excitation spectrum is shown in Fig. 4. As can be seen in Fig. 4, the spectrum and hence the velocity distribution is concentrated in a small region which corresponds to the initial velocity of the atoms. The small splitting in the line is due to the hyperfine structure of the $3P_{1/2}$ state. The fine-structure state change appears to happen with little or no change in velocity, justifying our assumption.

To calculate the signal amplitude we must determine $n_2(v)$, the velocity distribution of the $3P_{1/2}$ state. The equations describing this distribution and the longitudinal velocity distribution $n_4(v)$ of

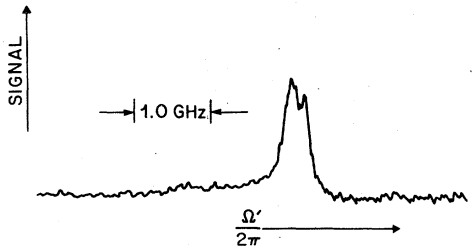

FIG. 4. Probe laser excitation spectrum of the $3P_{1/2} \rightarrow 4D_{3/2}$ transition with the pump laser tuned to the $3S_{1/2} \rightarrow 3P_{3/2}$ transition. This signal is the result of fine-structure state-changing collisions produced by 0.5 Torr of neon perturber gas. The narrow line width demonstrates that fine-structure state changes occur with negligible velocity change.

the $3P_{3/2}$ state are[11]

$$\frac{dn_2(v)}{dt} = -[\gamma_2 + \Gamma_2(v) + \gamma_{24}^t]n_2(v) + \gamma_{42}^t n_4(v) + \int W(v',v)n_2(v')dv' + T(v), \quad (4)$$

$$\frac{dn_4(v)}{dt} = -[\gamma_2 + \Gamma_2(v) + \gamma_{42}^t]n_4(v) + \gamma_{24}^t n_2(v) + \int W(v',v)n_4(v')dv', \quad (5)$$

where $T(v)$ is the velocity distribution of atoms excited to the $3P_{1/2}$ state by the pump laser. The collision kernel $W(v,v')$ is defined such that the $W(v,v')dv\,dt$ is the probability that a collision will cause an atom in level 2 moving with a longitudinal velocity between v and $v+dv$ to change to be between v' and $v'+dv$ during a time interval dt. The rate $\Gamma_2(v)$ is given by

$$\Gamma_2(v) = \int W(v,v')dv'$$

and $\gamma_{24}^t = \gamma^t$ and $\gamma_{42}^t = 0.5\gamma^t$ are the $3P_{1/2} \rightarrow 3P_{3/2}$ and $3P_{3/2} \rightarrow 3P_{1/2}$ collisional transfer rates, respectively.

The equation which gives $n(v) = n_2(v) + n_4(v)$, the longitudinal velocity distribution function for the sum of the population densities of the two $3P$ states, is

$$\frac{dn(v)}{dt} = -\left(\gamma_2 + \int W(v,v')dv'\right)n(v) + \int W(v',v)n(v')dv' + T(v). \quad (6)$$

Equation (6) is easily solved to yield the steady-state solution

$$n(v) = \sum_{i=0}^{\infty} n^i(v), \quad (7)$$

where

$$n^0(v) = T(v)/[\gamma_2 + \Gamma_2(v)],$$

$$n^{i+1}(v) = \int W(v',v)n^i(v')dv'/[\gamma_2 + \Gamma_2(v)].$$

The quantity $n^i(v)$ is the population density of atoms having experienced exactly i collisions since initially excited into the $3P$ states.

By substituting $n_4 = n - n_2$ into Eq. (4) and using Eq. (7), we solve Eq. (4) to obtain

$$n_2(v) = \sum_{i=0}^{\infty} n_2^i(v), \quad (8)$$

where

$$n_2^0(v) = \frac{0.5\gamma^t n(v) + T(v)}{\gamma_2 + \Gamma_2(v) + 1.5\gamma^t} \quad (9)$$

and

$$n_2^i(v) = \int W(v',v)n_2^{i-1}(v')dv'/[\gamma_2 + \Gamma_2(v) + 1.5\gamma^t]. \quad (10)$$

In this paper we consider two collision kernels for insertion into Eq. (10), the Keilson-Störer and the classical hard-sphere kernels. Owing to the simple mathematical form of the Keilson-Störer kernel an analytic expression for $n_2(v)$ can be obtained. However, for the hard-sphere kernel it is necessary to calculate $n_2(v)$ numerically. These collision kernels will be discussed in the following section. The distribution $n_2(v)$, given by Eqs. (8)–(10), is inserted into Eq. (3) and the total line shape is then given by Eqs. (1)–(3).

III. COLLISION KERNELS

All the properties of the velocity-changing collision process are contained in the collision kernel. The most commonly used kernel is the phenomenological kernel of Keilson and Störer[6]

$$W(v,v') = \Gamma[\pi(\Delta u)^2]^{-1/2}\exp[-(v' - \alpha v)^2/(\Delta u)^2],$$

where Γ is the (speed-independent) rate of collisions, α is a parameter which depends on the active and perturber atom mass ratio, and

$$\Delta u = (1 - \alpha^2)^{1/2}u$$

is $\sqrt{2}$ times the rms velocity change per collision. Borenstein and Lamb[12] compared the Keilson-Störer kernel with Monte Carlo calculations of hard-sphere collisions and found fairly close agreement between the two. However, they were concerned mainly with the cases of light perturbers and small initial velocities (velocities small compared with Doppler width). Recently, more detailed comparisons have been made[13,14] although again for cases of light perturbers and low velocities.

In this section we shall compare some of the properties of the Keilson-Störer kernel with the exact analytic expression for the kernel which describes classical collisions between atoms having a hard-sphere interatomic potential ($V = 0$ for $r > r_0$ and $V = \infty$ for $r < r_0$).

The Keilson-Störer kernel has the form of a displaced Gaussian whose width and shift are determined by the parameter α. The method for the determination of α which we utilize is that suggested by LeGouët,[13] in which α is chosen such that the Keilson-Störer model gives the same rms velocity change per collision as the analytic hard-sphere kernel. This method gives $\alpha = 0.8$,

0.4, and 0.0 for collisions between sodium and helium, neon and krypton atoms, respectively. A major feature of the Keilson-Störer kernel is its mathematical simplicity which allows analytic expressions to be obtained.

The hard-sphere kernel is considerably more complicated. It is given by the following expression:

$$W(v',v)=\frac{\pi r_0^2}{4}\left(\frac{1+\beta^2}{\beta^2}\right)\left(\left\{1-\mathrm{erf}\left[\left(\frac{1+\beta^2}{2\beta}\right)|S|+\beta\frac{v'}{u}\frac{S}{|S|}\right]\right\}\right.$$
$$\left.+\exp\left[-S\left(S+\frac{2v'}{u}\right)\right]\left\{1-\mathrm{erf}\left[\left(\frac{1-\beta^2}{2\beta}\right)|S|-\beta\frac{v'}{u}\frac{S}{|S|}\right]\right\}\right),$$

where

$$\beta^2=m_p/m_a,\quad S=(v-v')/u\,.$$

The mass of the active atom (Na) is m_a, and the mass of the perturber atom is m_p. This kernel has been obtained by Kol'chenko,[15] however, for completeness we have included its derivation in the Appendix.

To compare the kernels, we plot in Figs. 5–7 $n^i(v)$ [Eq. (7)] for sodium calculated with both kernels for helium, neon, and krypton perturbers assuming $T(v)$ is a delta function at $v/u=1.6$. In the case of a very light perturber such as helium (Fig. 5), the two kernels are quite similar. Each gives distributions $n^i(v)$ which shift more toward equilibrium with each collision, and both models produce distributions with approximately the same shifts and widths. To allow for easy comparison of the distributions we have normalized the peak of each to unity. In fact, at the pressure (2.5 Torr) used for the calculation, each sucessive $n^i(v)$ decreases in amplitude by about a factor of 6 or more.

The calculated distributions for the most massive perturber, krypton, show some significant differences. Krypton is 3.7 times heavier than sodium. As in the case of helium, the distributions predicted by the two kernels are quite similar for $i \geq 2$ although the widths of the distributions now predicted by the hard-sphere models are significantly larger than those given by the Keilson-Störer model owing to the speed dependence of $\Gamma(v)$ in the hard-sphere model. The greatest difference appears in the distribution $i=1$. Krypton hard-sphere collisions produce a relatively flat-topped distribution. The amplitude at $v=0$ is nearly the same as at the initial velocity (taken to be $v_0=1.6$ u). The Keilson-Störer distribution, on the other hand, is a factor of 12 larger at $v=0$ than at v_0. Note that the velocity distributions produced by the heavier perturber initially broaden and then narrow in the hard-sphere model, whereas for the Keilson-Störer kernel, complete thermalization occurs after one collision.

Comparisons of the distributions calculated using these two kernels indicate the following. First, for heavier perturbers it is at low pressures that the differences are most significant since it is at low perturber pressure that the contribution of $n^1(v)$ to $n(v)$ dominates. Second, for high perturber pressures the two kernels give nearly the same line shapes. Our experiments have therefore concentrated on fairly low per-

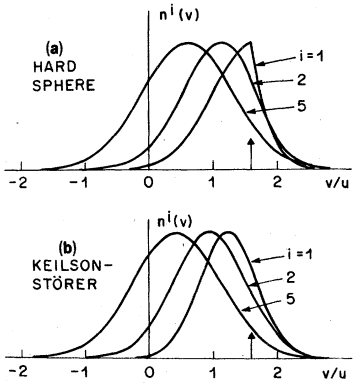

FIG. 5. The steady-state axial-velocity distributions $n^i(v)$ for sodium atoms in the $3P$ states which have experienced exactly i collisions since being initially excited. The calculations were carried out for 2.5 Torr of helium perturber gas, using both the (a) hard-sphere and (b) the Keilson-Störer kernels. All curves have been normalized to the same height.

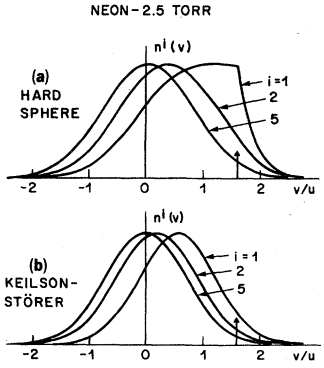

FIG. 6. Same as Fig. 5, except the perturber gas is neon.

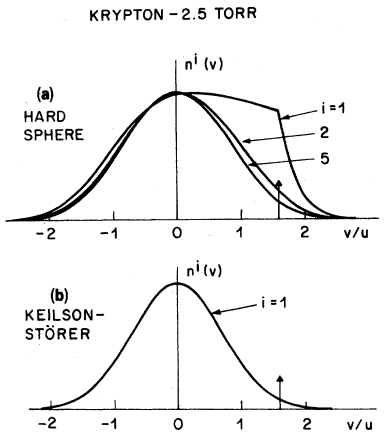

FIG. 7. Same as Fig. 5, except the perturber gas is krypton.

turber pressures. In the case of helium we expect the two models to give nearly identical results.

IV. EXPERIMENTAL RESULTS

Excitation spectra were taken of the $3S_{1/2} \rightarrow 3P_{1/2} \rightarrow 4D_{3/2}$ transition of atomic sodium vapor for various pressures of helium, neon, and krypton buffer gases. In each case, the laser at Ω was adjusted to be 1.6 GHz below the $3S_{1/2}(F=2) \rightarrow 3P_{1/2}$ transition. Examples of the spectra obtained by sweeping Ω' are given in Figs. 8–12. In each case, the two narrow line-shape features are the result of the combination of two-quantum and stepwise transitions originating from the two hyperfine levels of the ground state. The broader feature is the collision-induced signal and, as discussed earlier, arises from velocity-changed

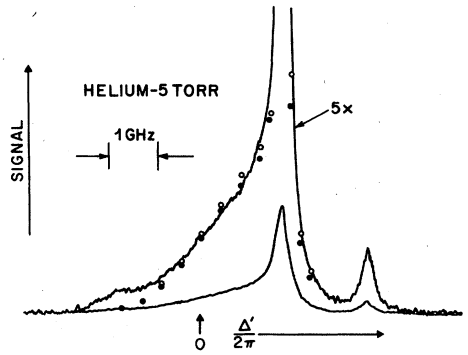

FIG. 8. Excitation spectrum of the $3S_{1/2} \rightarrow 3P_{1/2} \rightarrow 4D_{3/2}$ transition of atomic sodium in 5 Torr of helium perturber gas. The pump laser was tuned such that $\Delta/2\pi = -1.6$ GHz. The solid (open) circles show the theoretical fit obtained using the hard-sphere (Keilson-Störer) collision kernel.

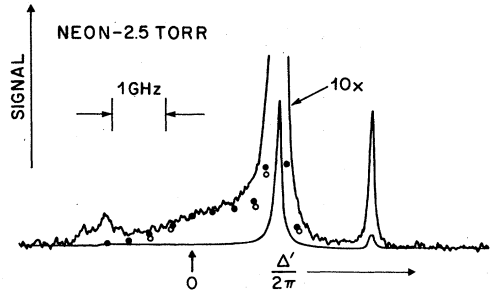

FIG. 9. Same as Fig. 8, except for 2.5 Torr of neon perturber gas.

atoms and atoms excited via phase-interrupting collisions. This feature is not present when the perturber gas is removed.

The excitation was made with counter-propagating beams. This geometry was utilized to minimize the line width of the two narrow two-photon and stepwise resonances. It is essential that these resonances be narrow so that the collision-induced signals are unobscured. If we use copropagating beams the narrow resonances are split by 390 MHz because of the hyperfine structure of the $3P_{1/2}$ state.[9] With the use of oppositely propagating beams, this splitting collapses[9] to 7 MHz. Some of the spectra contain evidence of resonances due to copropagating beams. These are symmetrically located about $\Delta' = 0$ from the counter-propagating resonances and apparently are the result of stray reflections into the sodium cell. We were unable to eliminate them completely.

We choose to set $\Omega/2\pi$ to be 1.6 GHz below the

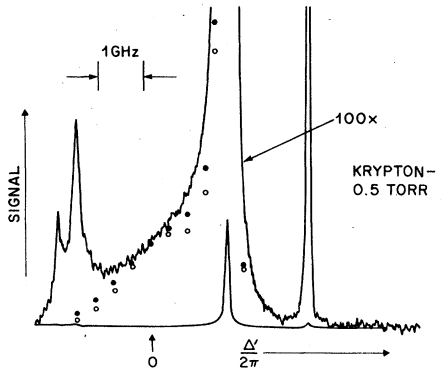

FIG. 10. Excitation spectrum of the $3S_{1/2} \rightarrow 3P_{1/2} \rightarrow 4D_{3/2}$ transition of atomic sodium in a perturber gas of krypton. The pump laser was tuned such that $\Delta/2\pi = -1.6$ GHz. The krypton pressure was 0.5 Torr. The solid (open) circles show the theoretical fit obtained using the hard-sphere (Keilson-Störer) collision kernel. The sharp resonances occurring for negative Δ' are due to the residual copropagating light, as discussed in the text.

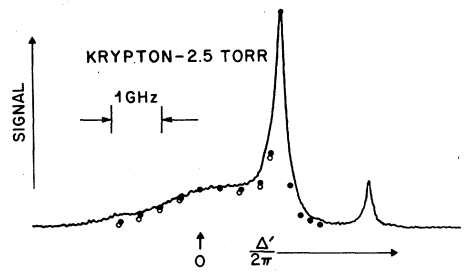

FIG. 11. Same as Fig. 10, except the krypton pressure was 2.5 Torr.

$3S_{1/2}(F=2) \rightarrow 3P_{1/2}$ transition. With this rather large detuning, the difference between the Keilson-Störer and hard-sphere kernel which we discussed in Sec. III is emphasized. Furthermore, the spurious copropagating resonances mentioned above are less troublesome since they occur at the edge of the line shape of interest. At this detuning the collisional redistribution and velocity-changing contributions to the line shape (components *b* and *c* of Fig. 2) are comparable in amplitude.

The data were fit to Eqs. (1)–(3) and (8)–(10) using experimental values of γ_{ij} and γ^t obtained from the literature,[16] and a value $\chi/ku = 0.018$ determined from measurements of pump intensity. The line shape was assumed to arise as an independent sum of contributions originating from both hyperfine ground states. The relative amplitudes of the two-narrow resonances were found to be pressure and intensity dependent. This dependence is due to optical-pumping effects which modify the population of the ground-state hyperfine levels. To account for the optical pumping, the initial relative population of the two states was taken as a free parameter which was adjusted so that the theory correctly predicted the relative amplitudes of the two narrow resonances.

The only remaining parameter to be determined is the velocity-changing collision cross section. We obtain values for these cross sections at each perturber pressure by fitting the ratio of the signal at $\Delta' = 0$ to that at $\Delta'/2\pi = 1.6$ GHz. Having fit these two ratios, the overall comparison between the theoretical and experimental profiles can be used to test various collision models. One should note that, for our procedure, the nature of the fit is relatively insensitive to the saturation parameter. This result was verified experimentally by varying the pump power. In our analysis we set the branching ratio $\gamma_2'/\gamma_2 = 1$ for both $3P_{1/2} \rightarrow 3S_{1/2}$ $(F=1)$ and $3P_{1/2} \rightarrow 3S_{1/2}$ $(F=2)$ transitions and $\Gamma_1(v)$ to gas kinetic values. The net effect of such an arbitrary choice is to modify the saturation parameter, but, as noted above, this modification has little effect on our fitting procedure. Finally, the assumption of a weak probe field is reasonably well satisfied; signal strength was found to vary linearly with probe power.

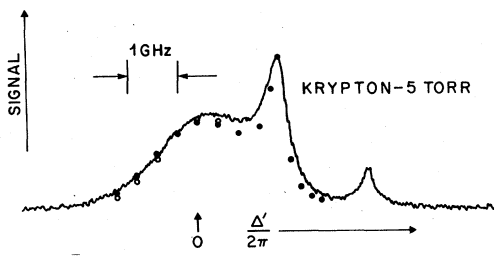

FIG. 12. Same as Fig. 10, except the krypton pressure was 5 Torr.

Representative data obtained with helium and neon buffer gases are shown in Figs. 8 and 9. The results of the theory using both the Keilson-Störer kernel (open circles) and the classical hard-sphere kernel (solid points) are given. As expected, for these lighter perturbers both kernels do nearly equally well in producing fairly accurate line shapes. However, for the data with krypton perturbers (Figs. 10–12) the hard-sphere model does better in predicting the line shape at the lowest pressure. The theoretical line shape using the hard-sphere kernel is slightly wider and gives more intensity in the region $\Delta'/2\pi = 1$ GHz than does the Keilson-Störer kernel and hence is in better agreement with the experimental data. Both models fail in the region very close to the narrow resonances.

To obtain curves which are more closely related to the velocity-changing collision kernel, we have attempted to extract from the experimental spectra only that component arising from velocity-changing collisions (component *b* of Fig. 2). To extract this component we subtract from the experimental data the theoretical contributions from all other sources. The results of this subtraction are shown in Figs. 13 and 14 as n_{vc}. The smooth curve represents the experimental points after this subtraction. The solid points give the theoretical velocity-changing contribution using the hard-sphere kernel and the open circles give the same for the Keilson-Störer kernel. In Fig. 13 we show results for the case of helium perturbers at 9.5 Torr. As expected from our earlier discussion, both collision kernels give similar distributions and these are in good agreement with the experimental data. The data for krypton at 1 Torr are given in Fig. 14. In this case, the hard-sphere model is clearly superior to the Keilson-Störer approximation, which produces a line shape which is too sharply peaked at $\Delta' = 0$.

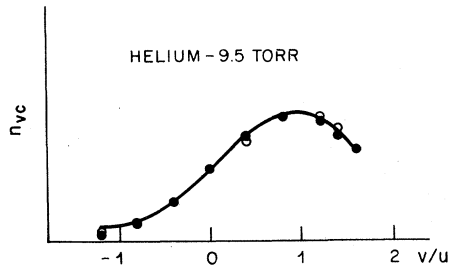

FIG. 13. The contribution of velocity-changing collisions to the excitation spectrum as a function of normalized velocity for 9.5 Torr of helium perturber gas. The smooth curve is the difference between the experimental excitation spectrum and the theoretical contributions to the excitation spectrum from all sources except velocity-changing collisions. The solid circles give the contribution due to velocity-changing collisions as calculated using the hard-sphere kernel; the open circles give the same for the Keilson-Störer kernel.

Although the hard-sphere calculation is in excellent agreement in the wing, it also fails for frequencies very near to the narrow resonance. Owing to the low pressure the theoretical line shapes in Fig. 14 are dominated by the $i=1$ contribution shown in Fig. 7.

The good agreement between theory and experiment in the line wings is evidence that large-angle scattering is correctly described by a hard-sphere model. This result is consistent with large-angle scattering occurring for very close collisions where the alkali–rare-gas potentials can be approximated by an infinite repulsive barrier. The failure of the theory near the narrow resonance for the heavier perturbers (Ne and Kr) is indicative of an interatomic potential that is other than hard sphere. Most likely there exist attractive wells in the Na*-Kr and Na*-Ne potentials that give rise to the additional scattering near the resonances.

The fact that the widths of the narrow resonance near $\Delta'/2\pi = 1.6$ GHz is generally larger than that predicted by the line-shape theory using empirically determined experimental values for all broadening parameters may be due to either (a) additional small-angle velocity-changing collisions or (b) larger values of the broadening parameters caused by the laser selection of fast Na atoms. We should also note that our theory of the $3P_{1/2} \rightleftharpoons 3P_{3/2}$ exchange is oversimplified and can lead to some additional errors.

The values for the hard-sphere collision cross sections which we obtain exhibit the pressure dependence shown in Fig. 15. The slow increase of the cross sections with increasing pressures is another indication that the theory is failing to account properly for the true collisional interaction. This variation implies that with increasing pressure the amplitude of the resonance at $\Delta'/2\pi = 1.6$ GHz becomes increasingly overestimated by the theory leading to anomalously large values for the calculated collision cross sections. Whether this variation is due to our model for $3P_{1/2} \rightleftharpoons 3P_{3/2}$ collisions, to effects of weak velocity-changing collisions, or to our failure to use speed-dependent broadening parameters is unknown at present. It would seem reasonable to consider the cross sections we obtained as upper bounds for the true cross sections.

The cross sections for collisions with neon and krypton are approximately 30 and 55 Å^2, respectively, and are similar to the values which can be deduced from ground-state gas kinetic radii.[17] The fact that the krypton cross section is larger is reasonable in light of its larger size and greater polarizability. The helium cross section of ~60 Å^2, on the other hand, does not fit this picture. The apparent helium cross section is the largest of the three measured cross sections within the estimated accuracy of our measurements of 30 to 40 percent despite the fact that the helium core is surely the smallest and the atom is the least polarizable. It should be noted, however, that we

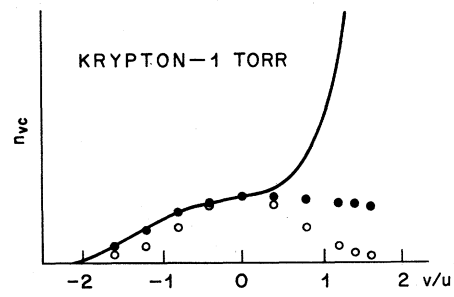

FIG. 14. Same as Fig. 13, except for 1 Torr of krypton perturber gas. The hard-sphere and Keilson-Störer kernels now lead to significantly different profiles.

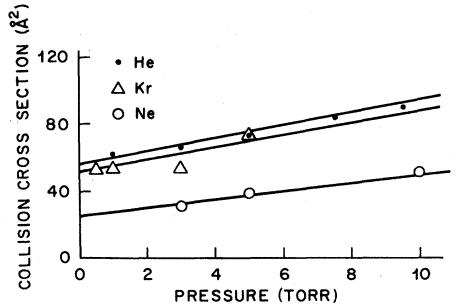

FIG. 15. Variation of the experimentally deduced cross sections for velocity-changing collisions between Na ($3P_{1/2}$) and He, Ne, and Kr perturbers as a function of perturber pressure.

have arbitrarily chosen to fit the data at $\Delta=0$, where, because of the small velocity change produced by sodium-helium collisions, the contribution of the velocity changing signal (component b in Fig. 2) is extremely small. Small errors in the calculation of component c will then result in substantial error in our result for the cross section. If instead, we fit the lowest-pressure helium data at $\Delta'/2\pi=1$ GHz, we find $\sigma=35$ Å^2, in better relative agreement with our expectations. However, the optimum cross section is still found to increase with pressure since the cross sections calculated at higher pressures are independent of where we fit the data.

V. CONCLUSION

We have examined the effects of velocity-changing collisions on the $3S_{1/2}\rightarrow 3P_{1/2}\rightarrow 4D_{3/2}$ excitation spectra of sodium vapor. The observed line shapes are reasonably well described by a theory in which collisions are characterized by either the phenomenological Keilson-Störer kernel or a classical hard-sphere kernel. For collisions between excited sodium atoms and heavy rare-gas atoms, the hard-sphere kernel is superior to the Keilson-Störer kernel. It gives a better description of the effects of large-angle scattering, although neither kernel provides a fully adequate description over the entire profile. The two kernels give essentially the same line shape for low active atom to perturber atom mass ratio. They also agree at high pressures independent of the mass ratio. Our data indicate that improved models are required to accurately describe sodium–rare-gas collisions. By fitting our data we extract effective hard-sphere collision cross sections for collisions between sodium $3P_{1/2}$ atoms and helium, neon, and krypton perturbers.

ACKNOWLEDGMENT

The work of one author (PRB) was supported by the U. S. Office of Naval Research.

APPENDIX

In this appendix, collision kernels and rates for classical hard-sphere scattering are derived. The collision kernel $W(\vec{v}',\vec{v})$ gives the probability density per unit time for a collision with the perturber bath to change the velocity of an "active atom" particle from $\vec{v}'$ to $\vec{v}$ and is given by[7]

$$W(\vec{v}',\vec{v})=N\left(\frac{m_a}{\mu}\right)\int d\vec{v}_p' d\vec{v}_r' W_p(\vec{v}_p') v_r^{-1} \times\delta\left(\vec{v}_r+\frac{m_a}{m_p}\vec{v}'-\frac{m_a}{\mu}\vec{v}+\vec{v}_p'\right) \times\delta(v_r-v_r')\left|f(\vec{v}_r',\vec{v}_r)\right|^2 \quad \text{(A1)}$$

with

$$\vec{v}_r=\vec{v}-\vec{v}_p,\quad \vec{v}_r'=\vec{v}'-\vec{v}_p',$$

where m_a is the active atom mass, m_p is the perturber mass, μ is the reduced mass, $\vec{v}$ (or $\vec{v}'$) is the active atom velocity, $\vec{v}_p$ (or $\vec{v}_p'$) is the perturber velocity, $|f_i(\vec{v}_r',\vec{v}_r)|^2$ is the differential scattering cross section, N is the perturber density, and $W_p(\vec{v}_p)$ the perturber velocity distribution assumed to be of the form

$$W_p(\vec{v}_p)=(\pi u_p^2)^{-3/2}\exp(-v_p^2/u_p^2), \quad \text{(A2a)}$$

$$u_p^2=2kT_p/m_p, \quad \text{(A2b)}$$

where T_p is the temperature associated with the perturbers. The delta functions in Eq. (A1) guarantee conservation of momentum and energy in the collisions.

For classical hard-sphere scattering,

$$|f_i(\vec{v}_r',\vec{v}_r)|^2=r_0^2/4, \quad \text{(A3)}$$

where r_0 is the sum of active atom and perturber hard-sphere radii. Substituting Eq. (A3) into Eq. (A1) and performing the integrations over $\vec{v}_p'$ and $\vec{v}_r$, one can obtain the kernel

$$W(\vec{v}',\vec{v})=\frac{N\pi r_0^2 u_p}{\pi^{3/2}\alpha^2u^2S}\exp\left\{-\left[\left(S+\frac{\mu\vec{S}\cdot\vec{v}'}{m_aS}\right)^2/\alpha^2u^2\right]\right\}, \quad \text{(A4)}$$

where

$$\vec{S}=\vec{v}-\vec{v}', \quad \text{(A5)}$$

$$u=2kT_a/m_a, \quad \text{(A6)}$$

$$\alpha=2(\mu/m_a)(u_p/u), \quad \text{(A7)}$$

and T_a is the temperature characterizing the active atoms. The rate associated with this kernel is

$$\Gamma(\vec{v})=\int d\vec{v}'W(\vec{v},\vec{v}') =N\pi r_0^2\left\{\frac{u_p}{\sqrt{2}}\exp\left[-\left(\frac{v}{u_p}\right)^2\right] +\left[1+\tfrac{1}{2}\left(\frac{u_p}{v}\right)^2\right]v\Phi\left(\frac{v}{u_p}\right)\right\}, \quad \text{(A8)}$$

where Φ is the error function. Note that, as expected, for $v\gg u_p$, $\Gamma(v)\sim N\pi r_0^2 v$ and, for $v\ll u_p$, $\Gamma(v)\sim N\pi r_0^2(2/\pi^{1/2})u_p$.

In the text, we use a one-dimensional kernel

obtained from Eq. (A1) by averaging over an initial transverse velocity distribution

$$W_t(\vec{v}_t') = (\pi u^2)^{-1} \exp[-(v_t'^2/u^2)], \tag{A9}$$

with

$$\vec{v}_t' = \vec{v}' - v_z'\hat{z} \tag{A10}$$

and summing over all final transverse velocities

$$\vec{v}_t = \vec{v} - v_z\hat{z}\,. \tag{A11}$$

Thus, the one-dimensional kernel is defined by

$$W(v_z', v_z) = \int dv_t dv_t' W_t(\vec{v}_t') W(\vec{v}', \vec{v})\,. \tag{A12}$$

Substituting Eqs. (A1) and (A9) into (A12) and carrying out the tedious but straightforward integrations, one may obtain

$$W(v_z', v_z) = \tfrac{1}{4}\pi r_0^2 N \frac{(1+\beta^2)}{\beta^2}\left\{1 - \Phi\left(\frac{1+\beta^2}{2\beta} r|S_z| + \frac{v_z'}{u}\beta\frac{S_z}{|S_z|}\right) + \exp\left[-rS_z\left(rS_z + \frac{2v_z'}{u}\right)\right]\right.$$
$$\left.\times\left[1 - \Phi\left(\frac{1-\beta^2}{2\beta} r|S_z| - \frac{v_z'}{u}\beta\frac{S_z}{|S_z|}\right)\right]\right\}, \tag{A13}$$

where

$$\beta = u/u_p\,,$$
$$r = (\beta^2 + T_a/T_p)/(\beta^2+1)\,.$$

If $T_a = T_p$, then $r = 1$ and one arrives at Eq. (12) of the text.

The rate $\Gamma(v_z)$ defined by

$$\Gamma(v_z) = \int dv_z' W(v_z, v_z')$$

may be calculated as

$$\Gamma(v_z) = \pi r_0^2 N u_p\left(\left(\frac{v_z}{u_p}\right)\Phi\left(\frac{v_z}{u_p}\right) + \pi^{-1/2}\exp\left[-\left(\frac{v_z}{u_p}\right)^2\right]\right.$$
$$\left.\times\left\{1 + \pi^{1/2}\int_0^\infty \exp\left(-\frac{\beta^2 x^2}{(1+\beta^2)^2}\right)\cosh\left(\frac{2v_z x}{u_p(1+\beta^2)^{1/2}}\right)\left[1 - \Phi\left(\frac{x}{1+\beta^2}\right)\right]dx\right\}\right). \tag{A14}$$

Equations (A4), (A8), and (A13) have been derived previously by Kol'chenko.[15] As noted in the text,[11] the use of one-dimensional kernels in the theory of saturation spectroscopy is not strictly valid when the collision rates are speed dependent.

[1] T. W. Hänsch and P. E. Toschek, IEEE, J. Quant. Elect. 5, 61 (1969); P. W. Smith and T. W. Hänsch, Phys. Rev. Lett. 26, 740 (1971); R. Keil, A. Schabert, and P. Toschek, Z. Phys. 261, 71 (1973); I. M. Beterov, Y. A. Matyugin, and V. P. Chebotaev, Zh. Eksp. Teor. Fiz. 64, 1495 (1973) [Sov. Phys.—JETP 37, 756 (1973)].

[2] W. K. Bischel and C. K. Rhodes, Phys. Rev. A14, 176 (1976); C. Brechignac, R. Vetter, and P. R. Berman, Phys. Rev. A 17, 1609 (1978); J. Phys. Lett. (Paris) 39, L231 (1978); T. Mossberg, A. Flusberg, R. Kachru, and S. R. Hartman, Phys. Rev. Lett. 42, 1665 (1979).

[3] C. N. Bagaev, E. V. Baklanov, and V. P. Chebotaev, Pis'ma Zh. Eksp. Teor. Fiz. 16, 15 (1972) [JETP Lett. 16, 9 (1972)]; T. W. Meyer, C. K. Rhodes, and H. A. Haus, Phys. Rev. A12, 1993 (1975); P. Cahuzac, O. Robaux, and R. Vetter, J. Phys. B 9, 3165 (1975); A. T. Mattick, N. A. Kurnit, and A. Javan, Chem. Phys. Lett. 38, 176 (1976); P. Cahuzac, E. Marie, O. Robaux, R. Vetter, and P. R. Berman, J. Phys. B 11, 645 (1978).

[4] D. L. Huber, Phys. Rev. 178, 93 (1969); A. Omont, E. W. Smith, and J. Cooper, Astrophys. J. 175, 185 (1972); J. L. Carlsten and A. Szöke, Phys. Rev. Lett. 36, 667 (1976); J. Phys. B 9, L231 (1976); J. L. Carlsten, A. Szöke, and M. G. Raymer, Phys. Rev. A 15, 1029 (1977); D. L. Rousseau, G. D. Patterson, and P. F. Williams, Phys. Rev. Lett. 34, 1306 (1975); R. D. Driver and J. L. Snider, J. Phys. B 10, 595 (1977).

[5] P. F. Liao, J. E. Bjorkholm, and P. R. Berman, Phys. Rev. A 20, 1489 (1979).

[6] J. Keilson and K. E. Störer, Q. Appl. Math. 10, 243 (1952).

[7] P. R. Berman, Adv. At. Mol. Phys. 13, 57 (1977).

[8] P. R. Berman, P. F. Liao, and J. E. Bjorkholm, Phys. Rev. A 20, 2389 (1979).

[9] See, for example, J. E. Bjorkholm and P. F. Liao, Phys. Rev. A14, 751 (1976) and references therein.

[10]See, for example, I. M. Beterov and V. P. Chebotaev, Prog. Quant. Electr. 3, 1 (1974); R. Salomaa and S. Stenholm, J. Phys. B 8, 1795 (1975); 9, 1221 (1976).

[11]The use of a one-dimensional kernel is not strictly valid in cases where the collision rates are speed dependent. In order to reduce the equations to those of an effective one-dimensional problem in velocity space, one must be able to factor the density matrix into parts depending on the longitudinal and transverse velocity components. This factorization procedure fails for saturation spectroscopy with speed-dependent rates; the pump laser field excites a nonthermal longitudinal velocity distribution which is transferred, in part, to the transverse velocity distribution *via* the speed dependence in the collision rate (i.e., if one excites a "hot" longitudinal atom, part of this heat is transferred to the transverse velocity distribution *via* collisions). The errors introduced by using a one-dimensional kernel are probably not severe, considering the overall accuracy of the calculation.

[12]M. Borenstein and W. E. Lamb, Phys. Rev. A5, 1311 (1972).

[13]J. L. LeGouët, J. Phys. B 11, 3001 (1978).

[14]C. R. Borde, private communication.

[15]A. P. Kol'chenko, S. G. Rautian, and A. M. Shalagin, Nucl. Physics Institute Semiconductor Physics Internal report, 1972 (unpublished).

[16]See Table I of Ref. 5.

[17]C. W. Allen, *Astrophysical Quantities*, 2nd ed. (Univ. of London, London, 1963), p. 45.